Estimated Seasonal Cycle of North Atlantic Eighteen Degree Water Volume

GAËL FORGET, GUILLAUME MAZE, MARTHA BUCKLEY, AND JOHN MARSHALL

Department of Earth, Atmospheric and Planetary Sciences, Massachusetts Institute of Technology, Cambridge, Massachusetts

(Manuscript received 18 March 2009, in final form 2 July 2010)

ABSTRACT

The seasonal cycle in the volume and formation rate of Eighteen Degree Water (EDW) in the North Atlantic is quantified over the 3-yr period from 2004 to 2006. The EDW layer is defined as all waters that have a temperature between 17° and 19°C. The study is facilitated by a synthesis of various observations—principally Argo profiles of temperature and salinity, sea surface temperature, and altimetry—using a general circulation model as an interpolation tool. The winter increase in EDW volume is most pronounced in February, peaking at about 8.6 Svy, where 1 Svy $\approx 3.15 \times 10^{13}$ m^3 corresponding to a 1 Sv (Sv $\equiv 10^6$ m^3 s^{-1}) flow sustained for one year. This largely reflects winter EDW formation due to air–sea heat fluxes. Over the remainder of the year, newly created EDW is consumed by air–sea heat fluxes and ocean mixing, which roughly contribute $^2/_3$ and $^1/_3$, respectively. The authors estimate a net annual volume increase of 1.4 Svy, averaged over the 3-yr period. It is small compared to the amplitude of the seasonal cycle (8.6 Svy) and annual formation due to air–sea fluxes (4.6 Svy). The overall EDW layer volume thus appears to fluctuate around a stable point during the study period. An estimate of the full EDW volume budget is provided along with an uncertainty estimate of 1.8 Svy, and largely resolves apparent conflicts between previous estimates.

1. Introduction

Mode waters are voluminous upper-ocean water masses characterized by near-homogeneous properties. The western subtropical North Atlantic contains a large volume of water with temperature close to 18°C, which has become known as Eighteen Degree Water (EDW). It is a characteristic feature that is typically found in the gyre recirculation to the south of the Gulf Stream. Attention was drawn to EDW by Worthington (1959), whose key contribution was to put EDW in the context of the large-scale ocean circulation and climate. Understanding the cycle of EDW formation and consumption is important because this water mass mediates heat exchange between the ocean interior and the atmosphere. Wintertime convection induced by surface cooling is thought to be the primary formation process. However, the precise nature of the formation/dissipation processes and their rates remain unclear and are the subject of vigorous research [e.g., the Clivar Mode Water Dynamic Experiment (CLIMODE), described in Marshall et al. (2009)]. In this context, the present study provides new insights into the seasonal fluctuation of EDW volume, based on the recent and extensive collection of Argo profiles.

Here, consistent with Worthington (1976), we simply define EDW as all fluid with a temperature between 17° and 19°C found in the Atlantic Ocean north of 5°N. The North Atlantic temperature distribution shows a mode in this temperature range: the so-defined EDW is therefore a mode water. A major advantage of such a simple definition is that the Walin (1982) framework can be applied to form a precise volume budget of the EDW layer. Let us emphasize, however, that there is no unique definition of EDW, and several flavors of EDW have been distinguished in the literature. Therefore, we will also discuss subsets of EDW that have low potential vorticity

$$\left(\mathrm{PV} = -\frac{f\,\partial\rho}{\rho_0 \partial z}\right)$$

and split EDW between the western basin and eastern basin (delimited by the 35°W meridian). The distinction of eastern and western EDW follows from Siedler et al. (1987), who designated eastern EDW as the ''Madeira Mode Water.''

Corresponding author address: Gaël Forget, Department of Earth, Atmospheric and Planetary Sciences, Massachusetts Institute of Technology, Cambridge, MA 02139.
E-mail: gforget@mit.edu

DOI: 10.1175/2010JPO4257.1

Two main approaches have been used to obtain observational insights into the volume budget of EDW: 1) volume census changes from in situ data (e.g., Worthington 1976; Kwon and Riser 2004) and 2) formation rates computed from air–sea fluxes (e.g., Worthington 1976; Speer and Tziperman 1992; Maze et al. 2009). Confusion has arisen because the two approaches yielded quantitatively different results, providing an important motivation for the CLIMODE project (see Marshall et al. 2009) and the present study. Errors associated with both approaches are likely to be very different, suggesting the utility of a combined methodology. One such is pursued here, allowing us to reconcile EDW volume and formation/dissipation rates by synthesizing the variety of available datasets within the dynamical framework of a general circulation model (GCM). Our broader goal is an improved dynamical and quantitative understanding of the seasonal cycle of EDW on the scale of the basin and its underlying mechanisms.

In section 2, we present the methods used to synthesize and analyze the observations, and characterize the seasonal cycle of the EDW layer. Our reference estimate of the full EDW volume budget is presented and analyzed in section 3. To place the full budget estimate in context and associate it with an uncertainty estimate, stand-alone estimates of a volume census based on Argo profiles and of surface formation rates from air–sea fluxes are assessed in section 4. The results shed new light on previous estimates, which we attempt to reconcile in section 5. Finally, section 6 summarizes and discusses the results.

2. Observational syntheses

a. Generalities

Our North Atlantic study exploits a recent near-global synthesis of the vast Argo, sea surface temperature, and altimetric datasets collected over the 3-yr period from 2004 to 2006 (Forget 2010). This dataset, the Ocean Comprehensible Atlas (OCCA), is obtained using GCM interpolation and consists of a time-varying estimate of the full ocean state. The 2004–06 period of analysis was chosen because of the unprecedented near-global in situ data coverage provided by Argo floats. By virtue of this relatively dense data coverage, the 2004–06 period ought to provide a good reference point to gauge past and future shifts in the ocean states.

Let us recall the motivation for using an ocean general circulation model (OGCM) as a data synthesis tool. A purely statistical model of the ocean behavior, based, for example, on a spatial decorrelation model, may be used to map Argo observations and estimate EDW volumes. However, there are at least three major, intertwined advantages in using GCM interpolation of the data, which are particularly relevant to EDW volume budget estimates. First, GCM interpolation is adequate to bring together the disparate variety of available observations and exploit their synergy. Second, GCM interpolation immediately yields full estimates of ocean budgets. Third, an OGCM is a convenient framework to carry out an extended interpretation of the observations in terms of known dynamical principles.

It is clear that neither statistical models nor OGCMs can yield perfect representations of ocean dynamics. When used to synthesize observations, both are susceptible to overfitting or underfitting observations, which may lead to a misinterpretation of the observations. To identify such occurrences and assess errors more generally, it is useful to compare results of different data synthesis methods. We will therefore also provide extensive comparisons between the OCCA estimate and data syntheses that do not involve an OGCM.

A crucial aspect of the data synthesis problem is how to deal with ''noise'' in the data due to aliasing of small-scale phenomena. Dynamical instabilities generating mesoscale or mixed layer eddies may be a key process in mode water dynamics, and such processes are accounted for by OGCMs (albeit in an imperfect, parametric form). It is clear, however, that the Argo array, despite vastly improving the in situ data coverage, cannot fully resolve the mesoscale and will alias eddy signals. It follows that the unresolved signals must be treated as data noise in the data synthesis process. In the syntheses presented below (whether using an OGCM or not) the data are accordingly smoothed in time and space. Let us now provide specifics on the data synthesis methods.

b. OCCA state estimate

The state estimation problem and methods that lead to the OCCA estimate are discussed in detail by Forget (2010). Briefly, a GCM–data synthesis is obtained as an approximate solution to a constrained nonlinear least squares estimation problem. The general circulation model employed is the Massachusetts Institute of Technology GCM (MITgcm) (Marshall et al. 1997; Adcroft et al. 2004) in the Estimating the Circulation and Climate of the Ocean (ECCO) framework (Stammer et al. 2002; Wunsch and Heimbach 2007) with a grid resolution of 1° horizontally and 50 levels in the vertical. The subgrid-scale processes are parameterized as background vertical mixing ($\mathcal{K} = 10^{-5}\,\mathrm{m^2\,s^{-1}}$), isopycnal mixing ($\mathcal{K} = 1000\,\mathrm{m^2\,s^{-1}}$), boundary layer vertical mixing [*K*-profile parameterization (KPP) scheme; Large et al. 1994], and a bolus velocity representing advection by eddies [Gent and McWilliams 1990 (GM) scheme, $\mathcal{K}$=1000 $\mathrm{m^2\,s^{-1}}$]. Air–sea fluxes are computed (from the

GCM) using the Large and Yeager (2004) algorithm, an adjusted version of National Centers for Environmental Prediction (NCEP) atmospheric state variables, and the GCM fields of SST (for details, see Forget 2010).

In the GCM, time-evolving fields are made to fit to a variety of observations (including Argo profiles, SST, and altimetric data), by iteratively adjusting initial conditions and surface forcing fields, using the adjoint method. The aforementioned mixing parameters are held constant, however. The 3-yr period from 2004 to 2006 is split into three 16-month overlapping time intervals. The choice of the estimation interval(s) of 16 months is a practical means to mitigate the effect of model error accumulation and yields a close fit to the observations. Each 16-month solution is required to strictly satisfy the GCM dynamics, but, when compiling the 3-yr time series, this strict constraint is relaxed over the periods when solutions overlap one another (for details, see Forget 2010).

The resulting estimate of the time-evolving ocean state (OCCA) closely matches Argo, SST, and altimetric observations over the 3-yr period from 2004 to 2006, within random error bounds (see Figs. 3–8 of Forget 2010). OCCA thus potentially provides robust observational estimates of water mass properties and volumes, which indeed will be established below for EDW (see sections 2d and 4a). In addition, OCCA includes estimates of air–sea fluxes and interior ocean fluxes that are constrained by ocean observations within the GCM interpolation framework. This yields a full EDW volume budget estimate (section 3), which along with the associated error estimate (section 4c) is the main result of our study.

c. EDW sample census method

To assess the reliability of OCCA estimates of EDW volumes, we shall compare them with the results of a very different data synthesis method, which we refer to as sample census (SC). It is based on a simple statistical model rather than a GCM.

For a given control volume $\mathcal{V}$, assume that N observations of temperature are available that are irregularly distributed within $\mathcal{V}$. The EDW volume V_{EDW} of fluid such that $17^\circ < T < 19^\circ$C in $\mathcal{V}$ is to be estimated. The sample census method consists of 1) computing the ratio $R_{\mathrm{EDW}} = N_{\mathrm{EDW}}/N$, where N_{EDW} is the number of samples satisfying $17^\circ < T < 19^\circ$C in $\mathcal{V}$ and 2) computing V_{EDW} as $R_{\mathrm{EDW}}\mathcal{V}$. The method can readily be generalized to any other water mass definition. As noted by Siedler et al. (1987), who used such a method, the necessary assumption is that the data coverage of $\mathcal{V}$ is sufficiently uniform to ensure that R_{EDW} is representative of the probability of finding EDW in $\mathcal{V}$. It is clear that this is an imperfect statistical model in the case of Argo profiles, which are rather irregularly distributed in space and time.

In practice, when dealing with a vast domain in this fashion, one should aim to appropriately split $\mathcal{V}$ into elementary control volumes $\{\mathcal{V}^i\}$ and estimate V_{EDW} as $\sum_i R^i_{\mathrm{EDW}}\mathcal{V}^i$, so as to minimize artifacts due to irregular sampling. Ideally, each $\mathcal{V}^i$ should be 1) large enough to contain numerous observations and 2) homogeneous enough to minimize irregular sampling within $\mathcal{V}^i$. In this study we use winter SST contours and depth levels to guide our choice of control volumes. The rationale is that the winter SST is representative of the mixed layer temperature at the peak of convection when mode waters are formed. In particular, each $\mathcal{V}^i$ is delimited in the horizontal by two contours (SST $= \Theta^i \pm \Delta\Theta$) of the 3-yr mean Remote Sensing Systems (RSS)–Reynolds March SST map (see Fig. 1; top-right panel shows a plan view of $\mathcal{V}^i$ for $\Theta^i = 18^\circ$C). Setting $\Delta\Theta = 1$ K we compute V_{EDW} as $\sum_i R^i_{\mathrm{EDW}}\mathcal{V}^i\delta\Theta/\Delta\Theta$, where $\delta\Theta = \Theta^{i+1} - \Theta^i = 0.1$ K. The small $\delta\Theta/\Delta\Theta = 0.1$ ratio is designed to reduce the noise level in V_{EDW} by smoothing the $R^i(\Theta^i)$ curves. We do no such smoothing in the vertical or in time. Section 4a discusses the resulting SC estimates of V_{EDW}. We first display the SC results in the form of R^i_{EDW} sections (Figs. 4–7). These are very useful for descriptive purposes.

d. Observed evolution of the EDW layer

Before turning to a more quantitative analysis, it is important to present the observed signals. The outcropping of the EDW layer and its seasonal variation are shown in Fig. 1. Isotherms sweep back and forth over a 20° latitudinal range, migrating northward under spring and summer warming and southward in fall and winter. The distances involved are very large (see Fig. 1) and do not reflect migration of fluid parcels but, rather, diabatic processes changing the properties of surface water. A key feature associated with EDW formation is the opening up of a broad outcrop in February and March over the western part of the basin (top-right panel). The EDW outcrop area typically peaks in March as it reaches its southernmost location, at which point it is more than twice as large as the summer outcrop area.

Figures 2 and 3 show the time evolution of the temperature profile beneath this winter outcrop window. In both the western basin (Fig. 2) and the eastern basin (Fig. 3), the EDW layer rapidly thickens in winter as the mixed layer deepens and reaches the preexisting subsurface EDW reservoir. In summer, the EDW layer gradually thins as the water column restratifies from the surface downward. The main difference between the two regions is that the EDW layer is shallower and thinner in the eastern basin (Fig. 3) than it is in the western basin

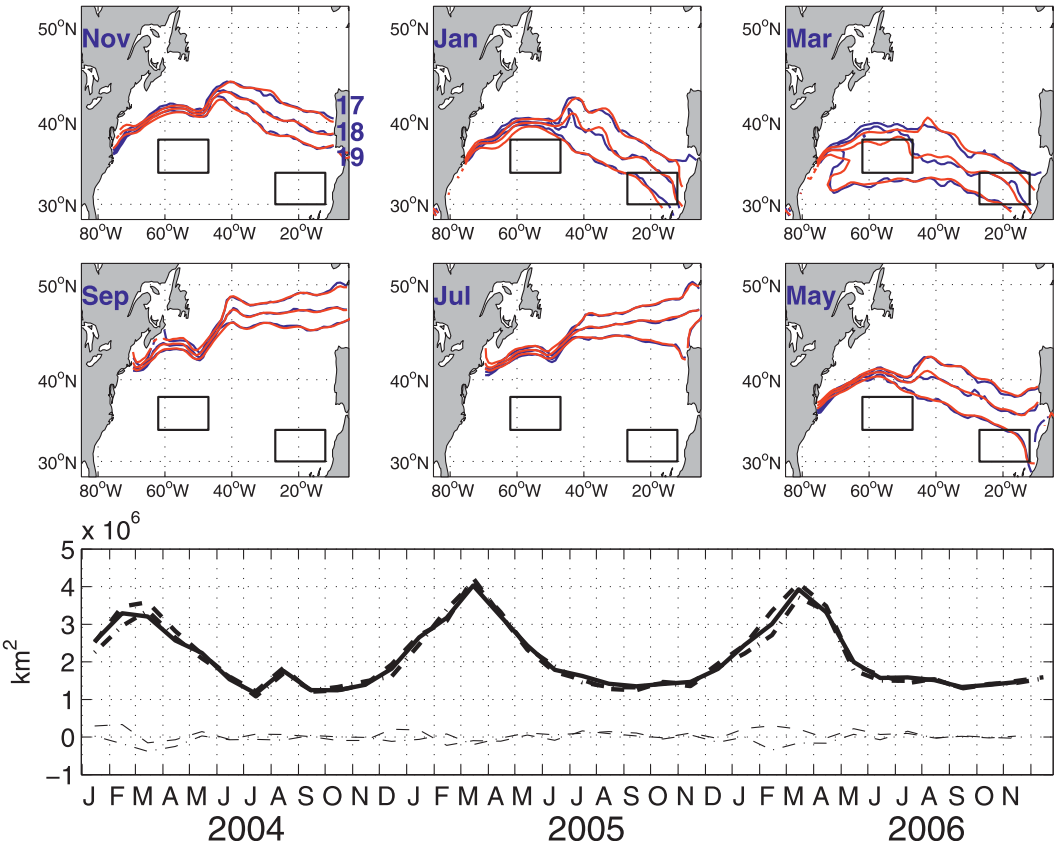

FIG. 1. (top), (middle) Mean monthly SST from two estimates (color contours) for the period December 2003 through November 2006. Each of the six panels represents a month of the year, forming a clockwise sequence. Only the 17°, 18°, and 19°C isotherms are shown. Blue contours are the average of mapped microwave SST data (RSS product) and mapped infrared SST data (Reynolds product), RSS–Reynolds SST. Red contours are OCCA mapped data (Forget 2010). The boxes used in Figs. 2 and 3 are shown in black. (bottom) Area of the 17°–19°C outcrop (in km^2) as a function of time in the OCCA (thick solid line), RSS (thick dashed–dotted line), and Reynolds (thick dashed line) estimates. The corresponding thin lines show the differences between OCCA and the two other estimates.

(Fig. 2). In the western basin, EDW typically occupies a depth range from 200 to 400 m in summer and 0 to 400 m in winter. The thickness of the EDW layer thus varies by a factor of 2 over the seasonal cycle, from 230 m at the peak of stratification to 430 m during winter convection. In the eastern basin these figures are typically smaller by a factor of 2. The thickness of the EDW layer varies by a factor of 3 over the seasonal cycle, but only from 50 to 180 m.

The evolution of the EDW layer below the surface is displayed in Fig. 4 using the sample census method (see section 2c). The figure shows the probability R_{EDW} that an Argo observation of T lies between 17° and 19°C, as a function of depth and "equivalent latitude."[1] In each panel of Fig. 4, for a given month of the year, the presence of EDW is indicated by R_{EDW} approaching unity. Figure 4 thus shows the southward (in fall and winter; top panels) and northward (in spring and summer; bottom panels) sweep of the EDW layer below the surface. In summer, the EDW layer exhibits a northward tilt near the surface. In winter, the EDW layer slopes strongly up to the surface, reflecting the downward penetration of the mixed layer. In March, the subsurface EDW reservoir (in the 150–400-m depth range) is connected directly to the surface through a well-mixed column. From March onward (bottom panels), the lower part of this "umbilical cord" becomes extended and eroded, while its upper part sweeps northward.

In exactly the same way, Figs. 5 and 6 show the evolution of two EDW subsets: EDW with potential vorticity, PV $< 1.5 \times 10^{-10}$ m^{-1} s^{-1} (Fig. 5), and EDW with PV $< 2 \times 10^{-11}$ m^{-1} s^{-1} (Fig. 6). The low PV restriction (PV $< 1.5 \times 10^{-10}$ m^{-1} s^{-1}) is guided by the literature

[1] The equivalent latitude of each elementary control volume $\mathcal{V}^i$ is defined as $L(\Theta^i) = \mathcal{A}^{-1}(A(\Theta^i))$, where $A(\Theta)$ is the area between the equator and the March SST $= \Theta$ contour, and $\mathcal{A}(\mathcal{L})$ is the area between the equator and the latitude $= \mathcal{L}$.

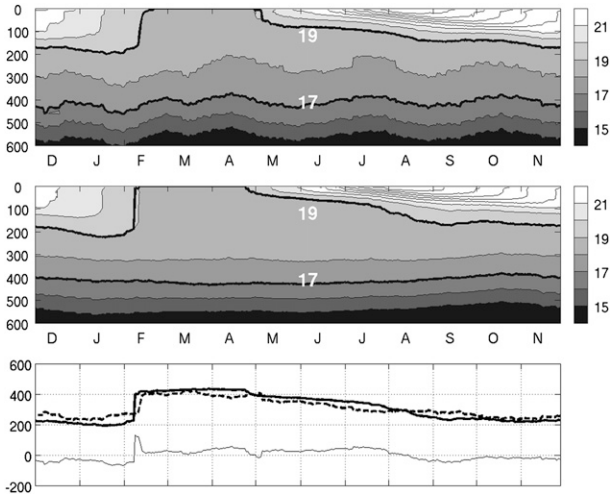

FIG. 2. Annual cycle of temperature (top) observed by Argo floats as a function of month and depth, averaged over the western box delimited by 34°–38°N, 62°–47°W (see Fig. 1) and averaged over the period from December 2003 through November 2006. A 1-month running window is used to bin average profiles. (middle) As in (top) but from OCCA fields sampled accordingly. EDW is defined as all fluid with temperature between 17° and 19°C. The thick black contours are the 17° and 19°C isotherms, marking the boundaries of the EDW layer. (bottom) The EDW layer thickness estimates (m) associated with the Argo profiles (thick dashed line) and the OCCA profiles (thick solid line). The thin solid line below shows the difference between the two estimates.

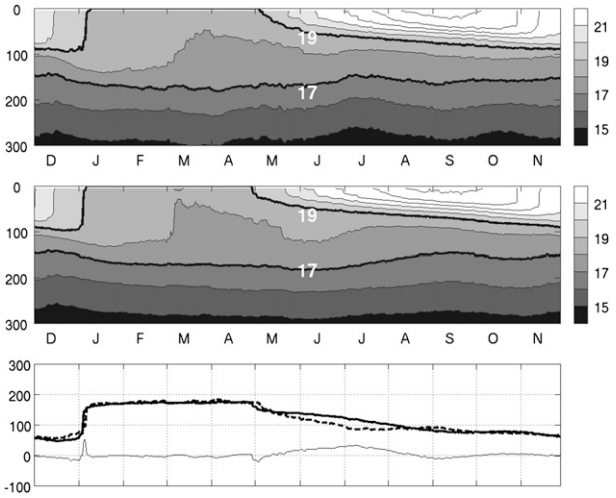

FIG. 3. As in Fig. 2 but for the eastern box (delimited by 30°–34°N, 27°–12°W; Fig. 1). Note that the depth range is half that of Fig. 2.

on subtropical mode waters (see Hanawa and Talley 2001; Kwon and Riser 2004). The very low PV restriction ($PV < 2 \times 10^{-11}$ m^{-1} s^{-1}) will also prove insightful (see below).

Figure 5 shows a surface mixed layer (ML) patch of low PV EDW and a large subsurface reservoir of low PV EDW that merge in winter. The ML patch appears to deepen and migrate southward during fall and winter (top panels). Kinematically, this behavior can be understood as follows: At any location, in winter, the ML cools down progressively as it deepens (reaching into colder layers beneath), and the ML fluid will temporarily qualify as EDW when the ML reaches the 18°C isotherm at this location. The ML temperature simply crosses the 18°C mark earlier at higher latitudes, where it was shallower in summertime (see Fig. 4). Hence, we observe a southward migration of the ML patch in winter (Fig. 5). In March the ML has reached the depth of the EDW reservoir, and the ML patch has reached its southernmost location. At this point, it cannot be distinguished from the EDW reservoir, which reaches right up to the surface. In spring and summer restratification proceeds downward from the surface (see Figs. 2, 3), increasing PV and causing the ML patch to progressively disappear, and the EDW reservoir returns to its prewinter subsurface configuration (Fig. 5). In the early fall, a new ML patch appears at the northernmost position of the EDW outcrop, initiating a new cycle.

Restricting attention to a very low PV subset of EDW allows one to focus on EDW that has recently been affected by convection in the ML (Fig. 6). The winter deepening and southward migration of the ML patch is thus most evident in Fig. 6. By March the ML is seen to penetrate the EDW reservoir down to a depth of 400 m, well into the core of the EDW reservoir, which resides at a depth of about 300 m (see Fig. 4). In May, after restratification has begun, very low PV EDW is left behind at the core of the EDW reservoir (Fig. 6, bottom right). It then progressively disappears reflecting its dissolution within the EDW reservoir. This behavior is suggestive of mixed layer deepening driving the EDW reservoir toward low potential vorticity.

Aside from their descriptive purpose, Figs. 1–6 also serve to test the reliability of ocean datasets (GCM interpolated or otherwise). First, the fact that individual datasets, prior to GCM interpolation, readily allow clear representations of EDW layer fluctuations is indicative of a rather solid database. In particular, the clear signals evident in Figs. 4–6 suggest that Argo provides the bulk of the in situ information needed to estimate the seasonal cycle of the EDW layer. It should be kept in mind, however, that the observational syntheses shown in Figs. 4–6 involve a stringent statistical model and a considerable amount of smoothing. Second, there is good agreement between OCCA and the datasets prior to GCM interpolation for both the time-varying surface outcrop (Fig. 1) and the time-varying vertical structure (Figs. 2, 3) of the EDW layer. Differences in the area

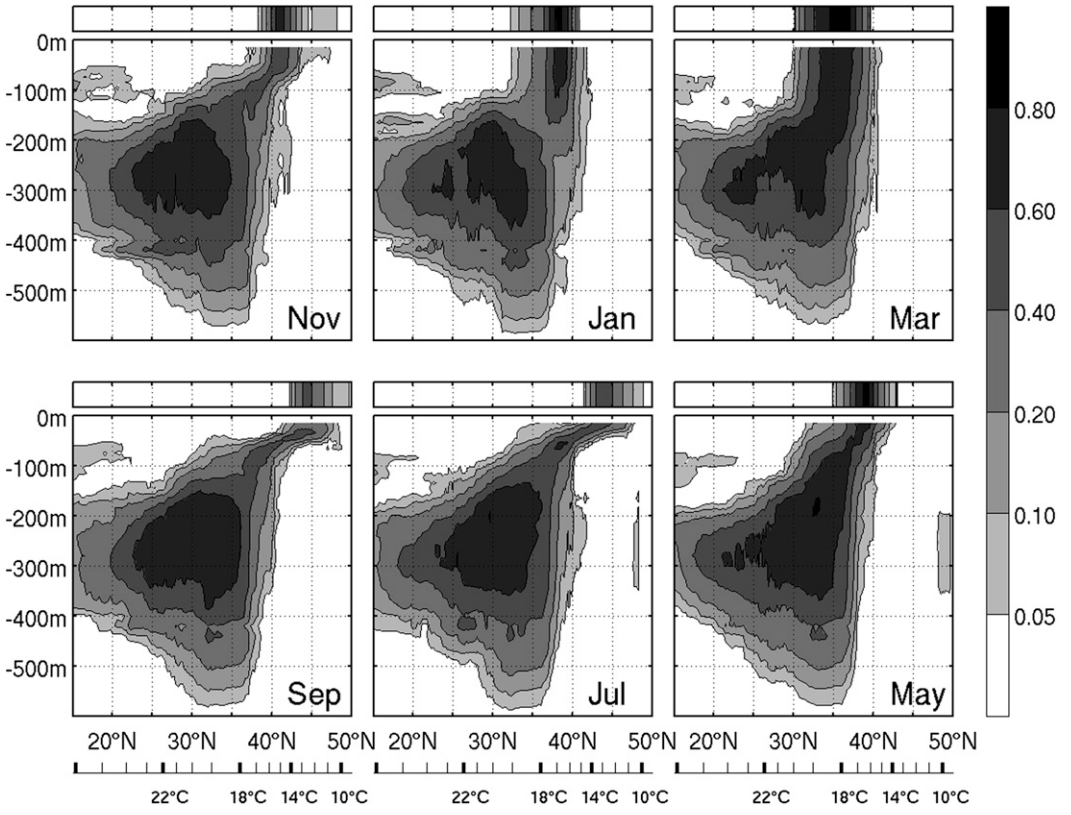

FIG. 4. Meridinal cross section of the average seasonal cycle of the EDW layer (over 2004–06) by applying the SC method to Argo profiles, as described in section 2c. The probability R^i_{EDW} that an Argo observation collected in a control volume $\mathcal{V}^i$ reveals EDW is plotted for the month indicated, as a function of the depth and equivalent latitude of $\mathcal{V}^i$. If $R^i_{\mathrm{EDW}} = 1$, then all observations collected in $\mathcal{V}^i$ satisfy the definition of EDW ($17° < T < 19°C$). Each $\mathcal{V}^i$ is delimited in the horizontal by two contours (SST $= \Theta^i \pm \Delta\Theta$) of the 3-yr-mean RSS–Reynolds March SST map (Fig. 1, top right). Both equivalent latitude $L(\Theta^i)$ and Θ^i are used as a horizontal axis. Equivalent latitude is defined as $L(\Theta) = \mathcal{A}^{-1}(A(\Theta))$, where $A(\Theta)$ is the area between the equator and the March SST $= \Theta$ contour and $\mathcal{A}(\mathcal{L})$ is the area between the equator and the latitude $= \mathcal{L}$. The bar at the top of each panel plots RSS–Reynolds SST in the same manner.

of the EDW outcrop (see Fig. 1, bottom) between the OCCA, Reynolds, and RSS SST maps have a standard deviation of 1.5×10^5 km^2, whereas the seasonal fluctuation is about 20 times larger. The correlation coefficients between the various estimates are close to 0.99. With regard to EDW layer thicknesses (see Figs. 2, 3, bottom), differences between OCCA and Argo estimates have a standard deviation of 40 m (12 m) for the western box (eastern box), while the seasonal fluctuation is five times (10 times) larger. The correlation coefficients between the various estimates are close to 0.95.

To further compare OCCA with Argo profiles, OCCA daily fields are sampled the same way as the Argo profiles, and a map of the fluctuating EDW layer is constructed using the SC method (see Fig. 7). A comparison of Fig. 7 (from OCCA profiles) and Fig. 4 (from raw Argo profiles) shows that the two representations of the fluctuating EDW layer are very similar. In particular, the features that were evident in Argo profiles (Fig. 4; prior to GCM interpolation) are consistently found in OCCA profiles (Fig. 7, after GCM interpolation). The same is true for the EDW subsets that are displayed in Figs. 5 and 6 (not shown). The most substantial inconsistency between OCCA profiles and raw Argo profiles is that the probability of finding EDW below 400 m, at the very bottom of the EDW layer, shows a low bias in Fig. 7 compared with Fig. 4 for all months of the year. As a result, we judge that the OCCA estimate for the annual-mean EDW volume (75 Svy) could be too small by perhaps 10%.

It should be kept in mind, however, that the Argo and SST datasets were made use of in OCCA (see Forget 2010), so the above consistency checks (using Figs. 1–7) should not be mistaken for comparisons of independent estimates. Instead, they demonstrate that OCCA is a rather adequate synthesis of Argo and SST data,

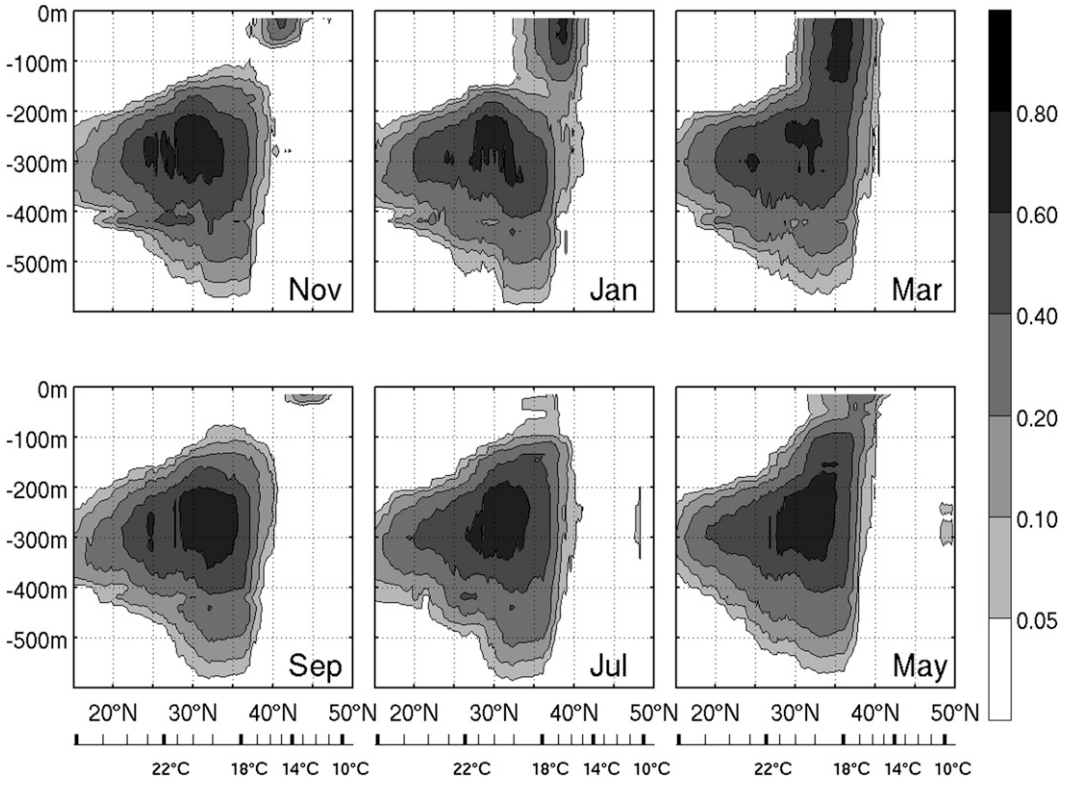

FIG. 5. As in Fig. 4 but for the subset of EDW with PV $< 1.5 \times 10^{-10}$ m^{-1} s^{-1} ($17° < T < 19°$C).

subject to the dynamical/thermodynamical constraints encoded in the GCM, and OCCA readily captures the signals of interest.

To complete this preliminary description, Fig. 8 reveals the time mean and variability of the EDW layer thickness using OCCA. We see that the mean EDW layer thickness is a maximum over a broad region to the southeast of the March 17°C isotherm (denoting the Gulf Stream path). The seasonal cycle in thickness is a maximum over the same broad region but appears to be slightly shifted to the northwest (right panel). Maxima in both thickness and thickness variation are well collocated with the opening of a broad winter outcrop, consistent with mode water being predominantly formed through a one-dimensional convective process. At lower latitudes, the EDW layer never outcrops and its thickness does not exhibit a strong seasonal cycle. The EDW layer remains relatively thick as far south as 20°N, however, which is more than 10° to the south of the winter outcrop region. This well-known feature of the EDW layer is suggestive of an influence of the EDW outcrop over a large fraction of the thermocline of the subtropical gyre. A secondary regional maximum in thickness variability is found in the eastern part of the basin, as first noted by Siedler et al. (1987). We now will quantify the seasonal cycle of EDW volume revealed in Figs. 1–8.

3. Estimated EDW volume seasonal cycle

a. Water mass transformation framework

The problem at hand is precisely formulated in the Walin (1982) framework. The volume budget of the EDW layer at time t within a control volume $\mathcal{V}$ (taken here as the North Atlantic north of 5°N) is written as

$$\frac{dV_{\mathrm{EDW}}}{dt} = \Delta A_{\mathrm{EDW}} - M_{\mathrm{EDW}}, \tag{1}$$

where $V_{\mathrm{EDW}}(t)$ is the volume of EDW in $\mathcal{V}$, $\Delta A_{\mathrm{EDW}}(t)$ is the "formation rate" of EDW in $\mathcal{V}$, and $M_{\mathrm{EDW}}(t)$ is the flow of EDW across 5°N (counted >0 out of $\mathcal{V}$, i.e., southward). Advection by mesoscale eddies, which is parameterized using the GM scheme, is included in $M_{\mathrm{EDW}}(t)$, and

$$\Delta A_{\mathrm{EDW}} = A_{19} - A_{17} \tag{2}$$

where A_{17} and A_{19} are the "transformation rates" A_Θ for $\Theta = 17°$C and $\Theta = 19°$C, that is, the volume fluxes through the 17° and 19°C isotherms (counted >0 toward colder isotherms). Thus, ΔA_{EDW} is the difference in the volume flux through the two (moving) isotherms that delimit the EDW layer (counted >0 if the EDW layer is

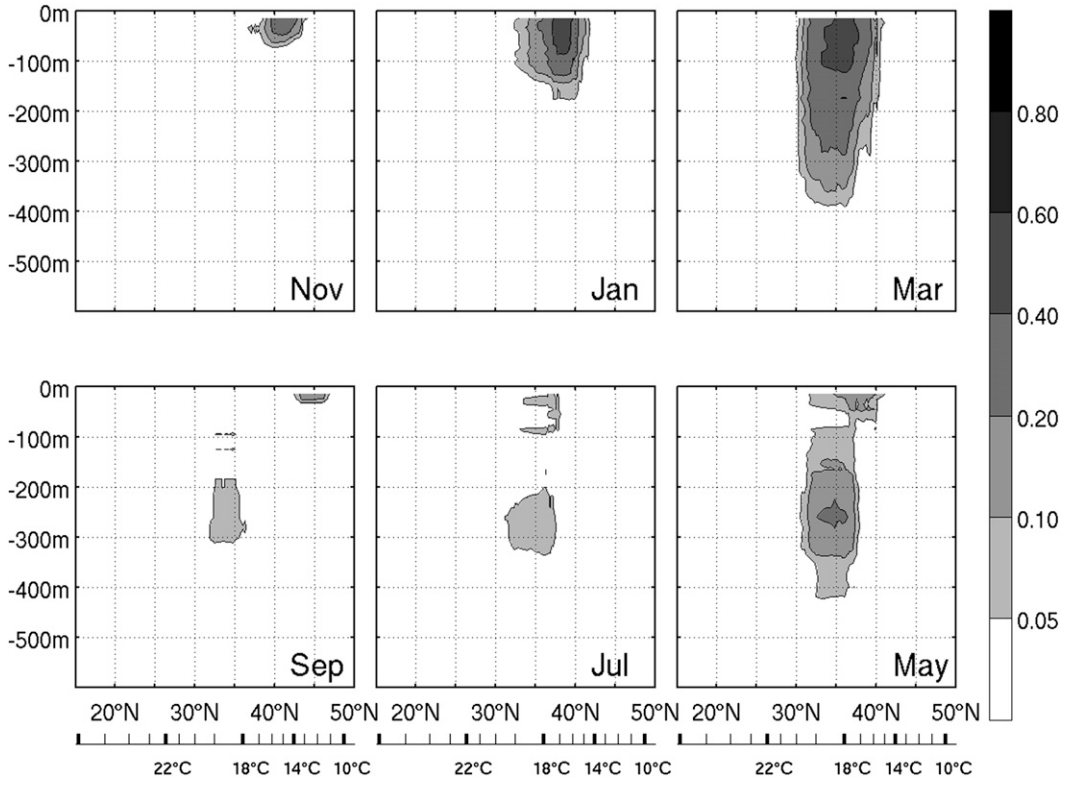

FIG. 6. As in Fig. 4 but for the subset of EDW with PV $< 2 \times 10^{-11}$ m^{-1} s^{-1} ($17° < T < 19°$C).

being inflated). We recall from Walin (1982) and studies that followed that

$$A_\Theta = \frac{\partial}{\partial \Theta}\left(\iiint_{R(\Theta,t)} -\frac{DT}{Dt}\, d\mathcal{V}\right), \tag{3}$$

where $R(\Theta, t)$ is the three-dimensional ocean region within $\mathcal{V}$ where $T < \Theta$ (increasing with Θ) and $DT/Dt = -\nabla \cdot \mathbf{N}_T$ is the convergence of nonadvective heat fluxes $\mathbf{N}_T$ (see, e.g., Marshall et al.1999). The ΔA_{EDW} may further be decomposed as

$$\Delta A_{\mathrm{EDW}} = \Delta A_{\mathrm{EDW,ext}} + \Delta A_{\mathrm{EDW,int}}, \tag{4}$$

where $\Delta A_{\mathrm{EDW,ext}}$ are external contributions due to air–sea heat fluxes, and $\Delta A_{\mathrm{EDW,int}}$ are internal contributions due to ocean mixing. So, $\Delta A_{\mathrm{EDW,int}}$ is the combined effect of vertical, isopycnal, and surface boundary layer diffusion. Here $\Delta A_{\mathrm{EDW,ext}}$ is not quite a sea surface term because shortwave fluxes can penetrate the subsurface. Equations (1)–(4) state that EDW volume fluctuations (dV_{EDW}/dt) consist of not only water mass transformations due air–sea fluxes ($\Delta A_{\mathrm{EDW,ext}}$) but also water mass transformations due to mixing ($\Delta A_{\mathrm{EDW,int}}$), and water mass fluxes out of the control volume (M_{EDW}). Comprehensive estimates of EDW volume fluctuations must address all four terms in Eqs. (1)–(4) and be obtained in an integrated fashion in compliance with Eqs. (1)–(4). Such an estimate, synthesizing the disparate variety of ocean datasets, is presented in section 3b.

b. OCCA reference estimate

Here we focus on the OCCA estimate for the 3-yr-average seasonal cycle in EDW volume. First, a 3-yr daily time series of Eqs. (1)–(4) is computed (see appendix for details). Second, the 2004, 2005, and 2006 daily rates are averaged together, leading to an average year daily time series (from $t_0 = 1$ December to $t_1 = 30$ November). Third, integrating in time leads to the average year daily time series of

$$\mathbb{V}_{\mathrm{EDW}}(t) = \overline{\Delta A_{\mathrm{EDW,ext}}}^{\,t} + \overline{\Delta A_{\mathrm{EDW,int}}}^{\,t} - \overline{M_{\mathrm{EDW}}}^{\,t}, \tag{5}$$

where $\mathbb{V}_{\mathrm{EDW}}(t)$ is the EDW volume at time t referenced to the EDW volume at time t_0 (i.e., 1 December) and the long overbar with superscript t denotes the time integral from t_0 to t. An equivalent notation for $\mathbb{V}_{\mathrm{EDW}}(t)$ is $\overline{dV_{\mathrm{EDW}}/dt}^{\,t}$. Results are presented in Sverdup–years (Svy), where 1 Svy $= 10^6 \times 365 \times 86\,400 \approx 3.15 \times 10^{13}$ m^3,

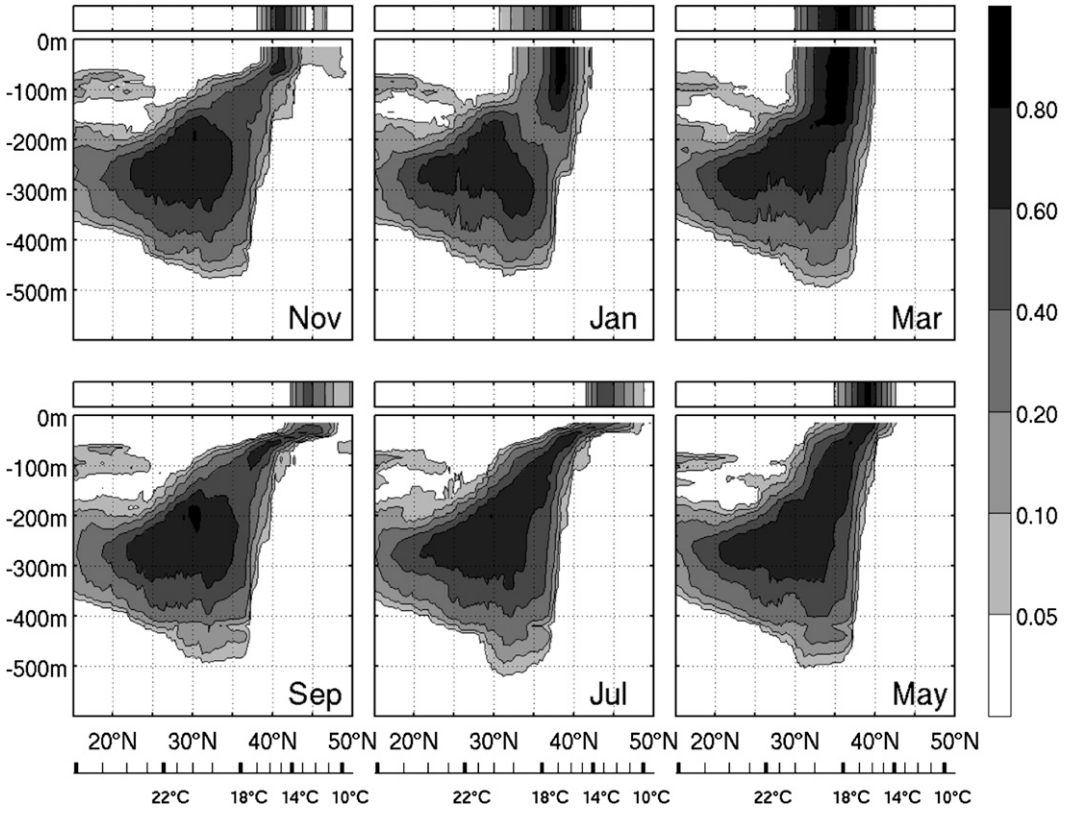

FIG. 7. As in Fig. 4 but for OCCA profiles (sampling OCCA daily fields accordingly) rather than Argo profiles. The bar at the top is now computed from OCCA SST maps.

corresponding to 1 Sv (Sv $\equiv 10^6$ m^3 s^{-1}) of volume flux sustained for one year.

A key advantage of the OCCA dataset is its representation of three-dimensional budgets of volume and heat, which allow diagnostic computation of a full volume budget for the EDW layer through Eq. (5). Nevertheless, numerical application of Eq. (5) is a nontrivial matter, which led us to use two different numerical recipes (see appendix). Using either recipe, the residual imbalances in Eq. (5) are three orders of magnitude less than the balancing terms.

Our reference estimate is displayed in Fig. 9. For each term in Eq. (5) it plots the interval between the two numerical recipes (shading) and the average result (thick curves). In this section, the estimates will be presented as $a \pm b$, where b is half the interval width; b quantifies uncertainties emerging from numerics alone and should not be mistaken as a full error estimate, which must also

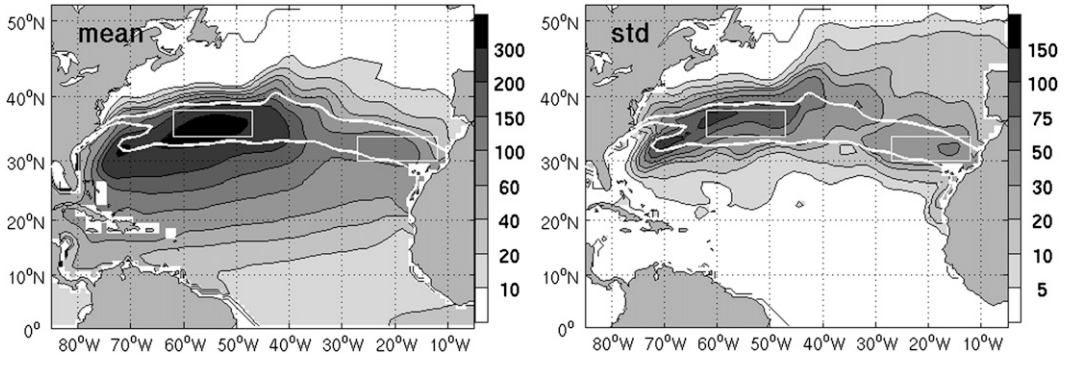

FIG. 8. (left) Time mean and (right) daily standard deviation of EDW layer thickness (m) for the 3-yr period from December 2003 through November 2006, using the OCCA dataset. The overlaid white contours are 1) mean March SST isotherms (17° and 19°C), using the OCCA dataset, and 2) the boxes used in Figs. 2 and 3.

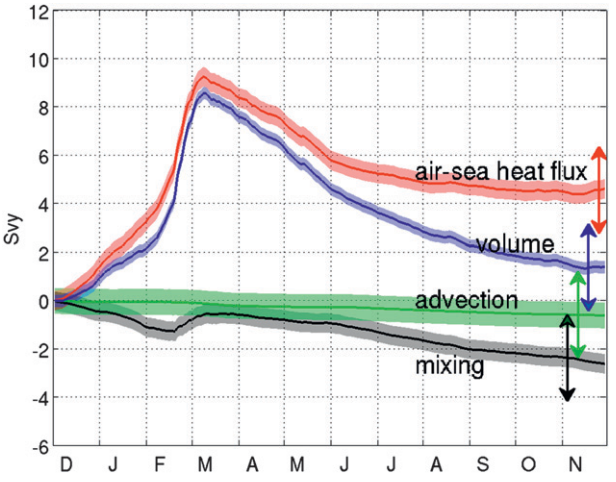

FIG. 9. Seasonal cycle in EDW volume for the average year, as estimated in OCCA over the 3-yr period from November 2003 through October 2006. The OCCA estimate of Eqs. (1)–(4) is displayed in the form of Eq. (5), the cumulative time integral from 1 December to 30 November of the average year. The blue line shows cumulated EDW volume change [$\mathbb{V}_{\mathrm{EDW}}$ in Eq. (5)]. The green line shows cumulated northward flow through 5°N ($-\overline{M_{\mathrm{EDW}}}^{t}$). The red line shows cumulated formation due to air–sea heat fluxes ($\overline{\Delta A_{\mathrm{EDW,ext}}}^{t}$). The black line shows cumulated formation due to ocean mixing ($\overline{\Delta A_{\mathrm{EDW,int}}}^{t}$). Two different recipes were used to diagnose Eq. (5) (see appendix). For each term in Eq. (5), the shading shows the interval between the two recipes, whereas the thick curve is the average of the two. Units: 1 Svy $\approx 3.15 \times 10^{13}$ m^3 corresponds to 1 Sv (Sv $\equiv 10^6$ m^3 s^{-1}) sustained for one year. The observational uncertainty estimate of section 4c is represented with arrows.

account for observational uncertainties (see section 4c and arrows in Fig. 9). Numerical uncertainties in EDW volume change $\mathbb{V}_{\mathrm{EDW}}$ amount to $2b = 0.5$ Svy by year end. Numerical uncertainties in EDW export $\overline{M_{\mathrm{EDW}}}^{t}$ amount to $2b = 1.1$ Svy by year end. These two combine to yield a numerical uncertainty of $2b = 1.6$ Svy in EDW formation $\overline{\Delta A_{\mathrm{EDW}}}^{t}$, which is split equally between $\overline{\Delta A_{\mathrm{EDW,int}}}^{t}$ and $\overline{\Delta A_{\mathrm{EDW,ext}}}^{t}$.

The EDW volume shows a rapid increase in winter to about 8.6 ± 0.3 Svy (relative to the 1 December value), achieving a maximum at the end of February. This mostly reflects the 9.3 ± 0.4 Svy wintertime formation by air–sea heat fluxes $\overline{\Delta A_{\mathrm{EDW,ext}}}^{t}$ due to vigorous cooling of the ocean. Subsequently air–sea heat fluxes consume 4.6 ± 0.4 Svy of the newly formed EDW mostly from March through May. The net annual effect of air–sea heat fluxes is a 4.6 ± 0.4 Svy formation of EDW. Mixing in the ocean interior $\overline{\Delta A_{\mathrm{EDW,int}}}^{t}$ consumes 2.6 ± 0.4 Svy by year end. It consumes EDW over most of the year, except in February when convective mixing tends to reinforce formation by air–sea heat fluxes (as denoted by the increase in $\overline{\Delta A_{\mathrm{EDW,int}}}^{t}$). The net total EDW formation (due to air–sea fluxes and mixing) hence is 2 ± 0.8 Svy. The EDW flux through 5°N is weakly southward throughout the year, only resulting in a 0.6 ± 0.6 Svy EDW export $\overline{M_{\mathrm{EDW}}}^{t}$ by year end. The net annual change in EDW volume $\mathbb{V}_{\mathrm{EDW}}$ is a relatively small increase of 1.4 ± 0.3 Svy yr^{-1} in the 3-yr average. The bulk of the estimated V_{EDW} interannual variability (±1.6 Svy, as reported in Table 1; see also section 4a) is due to this trend. The net total formation (2 ± 0.8 Svy) is balanced by volume change (1.4 ± 0.3 Svy) and, to a lesser extent, by a southward flow through 5°N (0.6 ± 0.6 Svy).

TABLE 1. Reference OCCA estimates (column 1) of the amplitude (peak to peak) of the average seasonal fluctuation in EDW volume (row 1) and various subsets (subsequent rows). Sensitivity tests are reported in columns 2–4, based on the sample census method (see section 2c; Fig. 10). The spread (reported below each estimate) is computed as the standard deviation of individual year monthly anomalies (from the 3-yr monthly average). Differences between columns 1 and 2 reflect the irregular Argo data coverage. Differences between columns 2–4 reflect different choices of smoothing/averaging. Unlike column 2, column 3 involves no preliminary smoothing of Argo profiles. Unlike column 2, column 4 involves no interannual variability of temperature, and the spread can only result from inhomogeneities in data coverage. Estimates are presented in Svy units (1 Svy $\approx 3.15 \times 10^{13}$ m^3).

	OCCA reference estimate	OCCA profiles	ARGO profiles	OCCA profiles (atlas)
All EDW	8.6 ±1.6	7.7 ±2.9	7.3 ±4.8	7.4 ±2.9
PV $< 1.5 \times 10^{-10}$ m^{-1} s^{-1}	15.5 ±2.0	11.1 ±2.9	9.3 ±5.8	14.4 ±3.1
PV $< 2 \times 10^{-11}$ m^{-1} s^{-1}	20.2 ±1.3	20.5 ±1.7	15.0 ±2.1	12.0 ±0.7
West of 35°W	7.6 ±1.4	7.1 ±3.0	7.3 ±4.7	7.6 ±3.0
East of 35°W	1.3 ±0.3	2.9 ±1.5	2.2 ±1.4	2.6 ±1.5

It is interesting to note that the net annual change in EDW volume (1.4 ± 0.3 Svy) is small compared with the seasonal fluctuation (8.6 ± 0.3 Svy). Gauging the EDW reservoir volume (75 Svy) with respect to this rate of annual volume change (1.4 Svy) implies a 50-yr time scale. The relatively large seasonal fluctuation, however, suggests that eight years may be sufficient to ventilate the EDW reservoir. The difference between these time scales is largely due to the restratifying effects of air–sea heat fluxes and mixing that balance wintertime creation. Although we do not exclude the possibility that seasonal cycle imbalances could be larger during other periods, the EDW volume appears to fluctuate around a rather stable point during 2004–06.

It should be emphasized that the annual formation by air–sea heat fluxes $\overline{\Delta A_{\mathrm{EDW,ext}}}^{t}$ alone does not yield

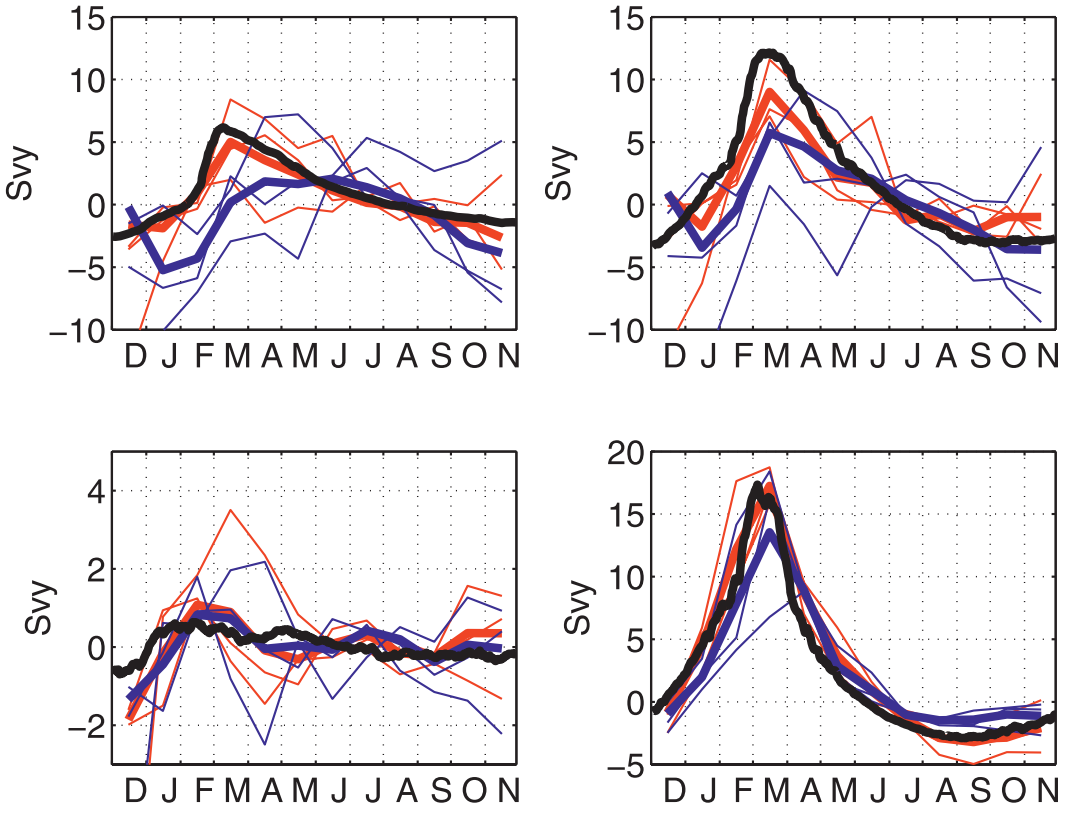

FIG. 10. Seasonal fluctuation obtained by SC of EDW (see section 2c for methodological details) in irregularly distributed Argo profiles (blue curves) or similarly sampled OCCA profiles (red curves). In each panel, the thick black curve is the corresponding reference OCCA estimate, based on complete daily fields rather than irregularly distributed profiles. Thick curves are for the 3-yr average and thin lines are for individual years: (top left) all EDW; (top right) EDW such that $|\mathrm{PV}| < 1.5 \times 10^{-10}$ m^{-1} s^{-1}; (bottom right) EDW such that $|\mathrm{PV}| < 2 \times 10^{-11}$ m^{-1} s^{-1}; and (bottom left) eastern basin EDW, located to the east of 35°W. For any curve of any panel, the median value has been subtracted. Units: Svy.

a good proxy for the annual volume change $\mathbb{V}_{\mathrm{EDW}}$. Neglecting the contribution of ocean mixing $\overline{\Delta A_{\mathrm{EDW,int}}}^{t}$ and, to a lesser extent, export $\overline{M_{\mathrm{EDW}}}^{t}$ would lead to an overestimation of the net annual volume change $\mathbb{V}_{\mathrm{EDW}}$ by a factor of 3 based on $\overline{\Delta A_{\mathrm{EDW,ext}}}^{t}$ alone. Wintertime air–sea heat fluxes, however, do largely determine wintertime volume change.

4. Sensitivity tests and uncertainty estimates

To put our reference estimate of the full EDW volume budget (Fig. 9) into perspective, we now consider stand-alone estimates of $V_{\mathrm{EDW}}(t)$ and $\overline{\Delta A_{\mathrm{EDW,ext}}}^{t}$. These sensitivity tests will provide insights into the different sources of uncertainty.

a. Sample census of EDW in Argo profiles

Stand-alone estimates of $V_{\mathrm{EDW}}(t)$ can be derived by an SC of EDW in Argo profiles (see section 2c). Volume estimates are obtained by computing volume-weighted integrals of the statistics shown in Fig. 4. This approach can be carried out with any set of profiles and water mass definition (e.g., for Fig. 5, 6, or 7). Monthly estimates of water mass volumes are thus shown in Fig. 10 for EDW or EDW subsets using Argo profiles or OCCA profiles (sampling OCCA fields as Argo did the real ocean). Thin lines denote individual year estimates (for 2004, 2005, or 2006), and thick lines denote the 3-yr-average estimates. We define the "spread" as the standard deviation of individual year monthly anomalies (from the corresponding 3-yr monthly average). Interpretation of this metric will be clarified below. Spreads and seasonal cycle amplitudes are reported in Table 1.

Let us start with the full EDW volume seasonal cycle, which is our main focus. The Argo SC estimate of EDW volumes (Fig. 10, top left: thick blue curve) shows a 7.3-Svy peak-to-peak seasonal cycle with a rapid volume increase in winter. This value is broadly consistent with the OCCA

reference estimate (thick black curve; 8.6 Svy) and the OCCA SC estimate (thick red curve; 7.7 Svy). This encouraging consistency suggests that Argo does provide a fairly solid database to estimate the EDW volume seasonal cycle over the period from 2004 to 2006 so that the result does not strongly depend on the choice of data synthesis method.

For SC estimates, the spread is relatively large, however: 2.9 Svy for OCCA profiles and 4.8 Svy for Argo profiles (see Table 1). It reflects systemic sampling errors (due to irregularities in data coverage) rather than robust signals of interannual variability. Indeed, when sampling OCCA as Argo does the real ocean, the spread in the OCCA SC estimate (2.9 Svy) becomes much larger than the spread in the OCCA reference estimate (1.6 Svy; based on full OCCA fields). Further evidence is given by the comparison of two OCCA SC results: 1) profiling daily fields that include interannual variability (Fig. 10, top left: red curves) and 2) profiling 3-yr-mean monthly fields that do not include interannual variability (not shown). The spread is the same in both cases (2.9 Svy; see Table 1), showing that the variation in data coverage suffices to explain this spread. Unsurprisingly, raw Argo profiles yield a larger spread (4.8 Svy) than do OCCA profiles (2.9 Svy). The former, indeed, include small/mesoscale signals that the float array cannot properly resolve, which is a large source of random noise. Hence, as expected, the smoothing provided by the coarse-resolution OGCM implies a clear spread reduction in SC estimates (from 4.8 to 2.9 Svy). Finally, the OCCA reference estimate spread (1.6 Svy; based on full OCCA fields) is the small fraction (11% in terms of variance) of the Argo SC spread (4.8 Svy) that may be due to large-scale interannual variability. Of course, this small fraction could also reflect an aliasing of "eddy noise," even though one may hope otherwise. Whether such interannual variability can rigorously be distinguished from noise is less than clear.

Before we turn to EDW formation by air–sea fluxes, let us examine SC results for subsets of EDW. The above conclusions generally hold for the various EDW subsets. They show similar temporal patterns (Fig. 10), and there is a satisfying quantitative agreement among the various estimates (Fig. 10 and Table 1), but SC results show a relatively large spread owing to sampling errors (Table 1). There are noticeable differences between the various EDW subsets, however, which are particularly relevant in the context of previous subtropical mode water studies, which have sometimes favored more restrictive water mass definitions. First, low PV restrictions tend to increase the seasonal cycle amplitude (Table 1, row 2 versus 1 and row 3 versus 2). The underlying reason seems clear: part of the lower PV EDW that is created during winter convection actually consists of preexisting EDW, whose PV gets reduced by convective mixing. This feature is most evident in Fig. 5 in the upper 100 m of the ocean where EDW is accounted for in winter, but discarded in summer when its PV is more than 1.5×10^{-10} m^{-1} s^{-1} (cf. Fig. 5 with Fig. 4). Second, the PV $< 1.5 \times 10^{-10}$ m^{-1} s^{-1} restriction tends to exacerbate sampling errors. For example, subsampling OCCA (as Argo sampled the ocean) leads to a 4.4-Svy offset in the case of EDW with PV $< 1.5 \times 10^{-10}$ m^{-1} s^{-1} (Table 1, row 2: column 2 versus 1). Also, the spread in the Argo SC estimate increases from 4.8 to 5.8 Svy upon introducing this PV restriction (Table 1, column 3: row 2 versus 1). The PV $< 2.0 \times 10^{-11}$ m^{-1} s^{-1} restriction seems more favorable in this respect. For this case, however, the smoothing provided by the OGCM implies a significant overestimation of the seasonal fluctuation (Table 1, row 3: column 2 versus 3). A closer investigation suggests that it is due to an offset in very low PV values (not shown). Finally, the seasonal fluctuation in EDW volume for the eastern basin is ~20% of the western basin value (Table 1, rows 4 and 5). While the western basin seasonal fluctuation is clearly predominant, the eastern basin provides a sizeable fraction of the total fluctuation (~15%, as noted by Siedler et al. 1987).

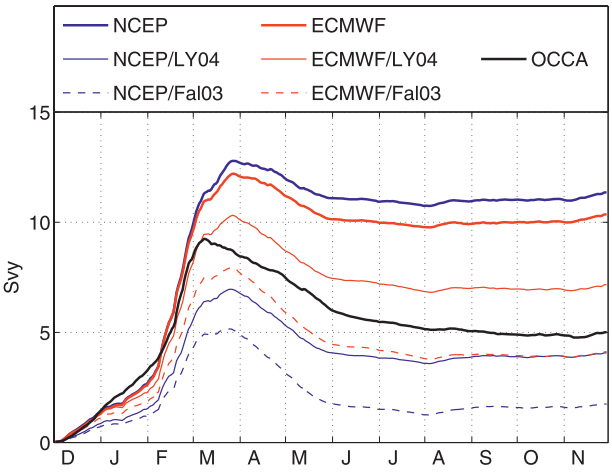

FIG. 11. Stand-alone estimates of cumulated EDW formation due to air–sea heat fluxes ($\overline{\Delta A_{\mathrm{EDW,ext}}}^{t}$) derived from NCEP and ECMWF data. In the legend, LY04 and Fal03 denote that the Large and Yeager (2004) and Fairall et al. (2003) bulk formulae algorithm was used to compute fluxes driven by reanalysis atmospheric state estimates. See section 4b for details. The reference estimate described in section 3b is plotted in black. Units: Svy.

b. EDW formation due to air–sea heat fluxes

We recall that OCCA air–sea fluxes are computed (from the GCM) using the Large and Yeager (2004) algorithm, an adjusted version of NCEP atmospheric

state variables, and the GCM fields of SST. The adjustment to NCEP fields is determined by the GCM interpolation procedure to best fit ocean observations (for details, see Forget 2010). The SST maps from Reynolds and Smith (1994) are applied as constraints (along with other ocean data) in that GCM interpolation procedure. The OCCA estimate of surface EDW formation rates is derived from the OCCA full temperature fields, along with the OCCA fluxes, using Eqs. (3) and (4).

Stand-alone estimates of surface EDW formation rates can be derived from atmospheric reanalysis datasets and SST maps, while omitting the available subsurface ocean observations. This is done using a simplified version of Eq. (3) for air–sea fluxes; that is,

$$A_{\Theta,\mathrm{ext}} = \frac{\partial}{\partial \Theta}\left(\iint_{S(\Theta,t)} \frac{Q_{\mathrm{net}}}{\rho_0 C_p}\, dS\right), \tag{6}$$

where $S(\Theta, t)$ is the sea surface within the control volume $\mathcal{V}$ in which $T < \Theta$, and $Q_{\mathrm{net}}/(\rho_0 C_p)$ is the net air–sea temperature flux directed out of the ocean (i.e., $Q_{\mathrm{net}} > 0$ is a cooling of the ocean, K m s^{-1}). The underlying simplification is that shortwave penetration is omitted, so computing Eq. (6) only requires SST fields (rather than full temperature fields). As in section 3b, the results are presented in the form of the time integrated EDW formation $\overline{\Delta A_{\mathrm{EDW,ext}}}^{t}$.

In Fig. 11, we thus show six stand-alone estimates of $\overline{\Delta A_{\mathrm{EDW,ext}}}^{t}$ that differ in the choice of reanalysis datasets (NCEP or ECMWF) and atmospheric surface layer parameterization. For each reanalysis, three sets of air–sea heat fluxes are considered, which correspond to three different atmospheric surface layer algorithms: (i) the reanalysis center algorithm; (ii) the Large and Yeager (2004) algorithm; and (iii) the Fairall et al. (2003) algorithm. In case (i) reanalysis maps of net air–sea heat flux (Qnet) are used. For (ii) and (iii) reanalysis maps of 10-m height state variables are used, along with Reynolds and Smith (1994) SST maps, to compute Q_{net} maps. Each of the six Q_{net} datasets is then used to compute $\overline{\Delta A_{\mathrm{EDW,ext}}}^{t}$ using Eq. (6) and Reynolds and Smith (1994) SST maps. Figure 11 is intended to complement the consideration of random errors presented by Maze et al. (2009) with an assessment of systematic errors. Since there is no clear consensus on the best combination of surface layer parameterization and reanalysis dataset, it is a priori unclear whether one of the six stand-alone $\overline{\Delta A_{\mathrm{EDW,ext}}}^{t}$ estimates is to be preferred. The intention here is not to argue for a particular one but to examine them as a group and assess the implied range of uncertainties.

It is encouraging that all estimates present the same overall temporal pattern in the seasonal cycle of EDW volume: winter formation followed by lesser spring consumption and almost no contribution in summer and fall. As pointed out by Maze et al. (2009), they also show good qualitative agreement in the spatial distribution of formation rates. Therefore, in these respects atmospheric reanalysis fields provide robust constraints on estimates of the full volume budget, such as the one discussed in section 3b. However, the stand-alone calculations imply wide ranges of estimates varying from 5 to 13 Svy for winter formation and from 2 to 11 Svy for net annual formation. Such wide ranges cannot be solely explained by the 1-Svy uncertainty in net annual formation estimated by Maze et al. (2009) due to random errors of moderate spatiotemporal correlation scales in meteorological fields. Further systematic errors are likely to arise owing to uncertainties in the bulk formulae coefficients and inconsistencies with chosen input fields. For example, we found that a 0.2×10^{-3} (i.e., ~15%) change in drag coefficient[2] is sufficient to imply a 1 Svy increase in annual EDW formation. Such uncertainties in the drag coefficient are likely to occur (see, e.g., Marshall et al. 2009).

Formation rates implied by OCCA air–sea fluxes happen to be in the center of the range of stand-alone estimates. We make no claim that OCCA air–sea fluxes are systematically more accurate than others. Unlike other datasets, however, they have been required to imply a seasonal fluctuation of the EDW layer that is consistent with ocean observations (as shown by Figs. 1–7, 10) and the GCM interior mixing rates.

c. Uncertainty estimate

We now derive an approximate uncertainty estimate for the reference OCCA estimate (of section 3b; Fig. 9), which is thought to reflect the limited availability of in situ observations. The 2.9 Svy spread among OCCA atlas SC results for the full EDW volume (Table 1, row 1, column 4) is taken as the uncertainty that prevails in individual-year monthly OCCA volume estimates. This value is regarded as quite a conservative estimate since 1) it discounts any additional skill that may be provided by other datasets (e.g., SST data) and dynamical constraints (i.e., the GCM) and 2) it implies that all of the interannual variability in the reference estimate (1.6 Svy) is noise. For 3-yr-mean monthly OCCA volume estimates, the uncertainty is then computed as $2.9/\sqrt{3} \approx 1.8$ Svy. Here the factor of $1/\sqrt{3}$ reflects that 3-yr-mean estimates

[2] Turbulent, sensible, and latent air–sea heat fluxes depend on the drag coefficient through the Stanton and Dalton transfer coefficients in the Large and Yeager (2004) bulk formulae algorithm.

TABLE 2. Previous and present estimates of EDW and subtropical mode water volumes, annual formation, and amplitudes of the seasonal cycle. Note that the various studies differ in water mass definitions. The second column shows the water mass definition depending on the author. The last column expresses volumes in Svy units (1 Svy $\approx 3.15 \times 10^{13}$ m^3).

Reference	EDW definition	Specifications	Value
Kwon and Riser (2004)	$17° < T < 19°$C $\partial T/\partial Z < 0.006°$C m^{-1}	Volume (western basin, winter)	12.5
Worthington(1976)	$17° < T < 19°$C	Volume (western basin, annual mean)	56
Worthington(1976)	$17° < T < 19°$C	Volume (full North Atlantic, annual mean)	80
This study, OCCA	$17° < T < 19°$C	Volume (full North Atlantic, annual mean)	75
Speer and Tziperman(1992)	$26 < \sigma < 27$ kg m^{-3}	Volume formed due to buoyancy flux (full North Atlantic) over a year	14
Speer and Tziperman (1992)	$26 < \sigma < 27$ kg m^{-3}	Volume formed due to heat flux (full North Atlantic) over a year	≈8
Worthington(1976)	$17° < T < 19°$C	Volume formed due to heat flux (western North Atlantic) over a year	7.3
This study, Maze et al.(2009), OCCA	$17° < T < 19°$C	Volume formed due to heat flux (full North Atlantic, annual mean)	4.6
Kwon and Riser (2004)	$17° < T < 19°$C $\partial T/\partial Z < 0.006°$C m^{-1}	Volume fluctuation (western basin, winter vs autumn)	3.5
This study, OCCA	$17° < T < 19°$C	Volume fluctuation (full North Atlantic, Mar vs Dec)	8.6

are based on roughly three times as many observations as individual-year estimates.

In theory, under an assumption of error independence, the error variance for $\mathbb{V}_{\mathrm{EDW}}(t)$ should equal the sum of error variances for the three terms on the rhs of Eq. (5). However we conservatively assume that any rhs term may be responsible for the full uncertainty in $\mathbb{V}_{\mathrm{EDW}}(t)$, rather than just a fraction of it. Hence, in Fig. 9, the arrows mark a $\pm$1.8-Svy error margin for $\mathbb{V}_{\mathrm{EDW}}(t)$ and also $\overline{\Delta A_{\mathrm{EDW,ext}}}^{t}$, $\overline{\Delta A_{\mathrm{EDW,int}}}^{t}$, and $\overline{M_{\mathrm{EDW}}}^{t}$.

Our error budget for Eq. (5) is conservative by design. Yet, it is very approximate and will eventually need to be refined. Unfortunately, we lack a practical method to carry out a full error budget of Eq. (5) at this stage. The crudeness of our present error estimate cannot be overstated, however, and should be kept in mind. There could be additional compensating errors on the rhs of Eq. (5). Moreover, there may be some seasonality in the error budget due to, for example, parameterized mixing processes, which are likely to be rather imprecise.

5. A discussion of previous estimates

a. Potential sources of inconsistencies

One of the main motivations for the CLIMODE observational program was the apparent conflict between previous stand-alone estimates of volume census changes (i.e., $\mathbb{V}_{\mathrm{EDW}}$) and formation by air–sea heat fluxes (i.e., $\overline{\Delta A_{\mathrm{EDW,ext}}}^{t}$). Table 2 summarizes estimates from representative studies. Here we begin by assessing potential sources of apparent conflicts using our own results. We will then attempt to reconcile previous estimates with one another and with those presented here.

First, large differences between $\mathbb{V}_{\mathrm{EDW}}$ and $\overline{\Delta A_{\mathrm{EDW,ext}}}^{t}$ estimates may not necessarily imply that they are in conflict. Indeed, Eq. (5) involves mixing ($\overline{\Delta A_{\mathrm{EDW,int}}}^{t}$) and export ($\overline{M_{\mathrm{EDW}}}^{t}$) terms in addition to $\mathbb{V}_{\mathrm{EDW}}$ and $\overline{\Delta A_{\mathrm{EDW,ext}}}^{t}$. Comparisons between estimates of $\mathbb{V}_{\mathrm{EDW}}$ and $\overline{\Delta A_{\mathrm{EDW,ext}}}^{t}$ must take these contributions in to account.[3] According to our reference estimate (section 3b), mixing and export can amount to 3.2 Svy. Neglect of these processes could thus lead one to wrongly conclude that estimates of formation by air–sea heat fluxes ($\overline{\Delta A_{\mathrm{EDW,ext}}}^{t}$) are, for example, three times too large compared with volume census change estimates ($\mathbb{V}_{\mathrm{EDW}}$).

Second, subjectivity in water mass definitions is a major potential source of confusion. There is never a single "best" water mass definition but a continuum of useful ones, and results can be very sensitive to subtle differences. For example, we found that adding potential vorticity restrictions tends to increase the amplitude of the seasonal cycle by up to a factor of 2 (Table 1, from row 1 to 2 to 3). Such a sensitivity should be kept in mind when comparing estimates discussed in the literature.

Third, uncertainties in $\mathbb{V}_{\mathrm{EDW}}$ and $\overline{\Delta A_{\mathrm{EDW,ext}}}^{t}$ estimates can be large. In particular, stand-alone estimates for $\overline{\Delta A_{\mathrm{EDW,ext}}}^{t}$ were found to differ by as much as a factor of 5. Such sensitivity can be translated to an error margin of $\pm(11 - 2)/2 = \pm 4.5$ Svy when a heat flux

[3] Of course, if errors in stand-alone estimates of $\mathbb{V}_{\mathrm{EDW}}$ and $\overline{\Delta A_{\mathrm{EDW,ext}}}^{t}$ were well known and small, differences between them would readily lead to useful inferences of the combined contribution of mixing and export. However, this is not the case at present.

dataset is simply selected from those available without making use of additional constraints from ocean observations. This, by itself, could explain apparent conflicts among previous estimates.

Fourth, estimates from the literature often differ in the time period under consideration. Low frequency variability thus provides another potential source of apparent conflict among published estimates. Whether it is significant compared with the aforementioned issues is less than clear, however. In our reference estimate, interannual fluctuations in EDW volume (i.e., anomalies from the Fig. 9 blue curve) have a standard deviation of 1.6 Svy. Hence, it is below the estimated level of random errors (±2.9 Svy for individual month EDW volumes), even though Argo provides a relatively dense data coverage over the studied period.

For our reference estimate (section 3b) the first two concerns are largely resolved by using self-consistent approaches to data synthesis and volume budget analysis. In this sense, estimates of volume census change ($\mathbb{V}_{\mathrm{EDW}}$) and formation by air–sea heat fluxes $\overline{\Delta A_{\mathrm{EDW,ext}}}^{t}$ are readily reconciled by our reference estimate. Furthermore, the second concern is mitigated by the fact that water mass definitions were only introduced at the analysis stage, whereas the data synthesis step (leading to OCCA) did not assume any. Hence, it is a simple matter to change our EDW definition in future studies and adjust our reference estimate accordingly. The third issue is addressed by attaching a reasonably conservative error estimate (section 4c) to our reference estimate (section 3b). Regarding the fourth concern, our results suggest that it is not a highly significant issue at this stage, as compared with the level of random errors.

It is clear that any data synthesis effort involves choices of methodology, each with its own source of systematic errors, and the present study is no exception. The impact of statistical and/or dynamical model errors is hard to fully evaluate. Comparing the results of different methods is the most practical, albeit approximate, approach, as carried out here in section 4. It was found that $\mathbb{V}_{\mathrm{EDW}}$ estimates for the 2004–06 period, especially those that do not involve PV restrictions (see Table 1, rows 1, 4, and 5), do not strongly depend on the choice of data synthesis method.

b. Reconciling previous estimates

Regarding net annual EDW formation $\overline{\Delta A_{\mathrm{EDW,ext}}}^{t}$ inferred from air sea fluxes, the estimates of Worthington (1976), 7.3 ± 4.5 Svy, and Speer and Tziperman (1992), 8 ± 4.5 Svy, are slightly larger than our reference value, 4.6 ± 1.8 Svy, but are well within error margins. The 4.5-Svy error margin that we place on estimates of Worthington (1976) and Speer and Tziperman (1992) seems appropriate because they selected a heat flux dataset from those available and made no use of additional constraints from ocean observations. We note that Worthington (1976) did not quantify errors for his estimate but envisioned that they would be very large. It may be fortunate that the Worthington (1976) estimate agrees so well with the other two. Regarding Speer and Tziperman (1992), we note that their total estimate (14 Svy) accounts for both freshwater and heat fluxes. To facilitate comparison with other estimates in Table 2, which omit salinity and freshwater fluxes, we tabulated their estimate from heat fluxes alone (~8 Svy) based on their Fig. 3. Finally, although the periods of the three estimates differ, there is no reason to invoke interannual variability to explain the differences between them, given the large systematic error margin (±4.5 Sv, see Fig. 11).

In respect to EDW volume fluctuations, Kwon and Riser (2004) estimate a seasonal cycle of 3.5 ± 0.5 Svy, whereas our reference estimate is 8.6 ± 1.8 Svy. The comparison of these two estimates is complicated by several factors. First, it is striking that Kwon and Riser focus on a small fraction (~⅕) of what Worthington and the present study refer to as EDW (see annual-mean volumes in Table 2). This likely explains why their estimate for the seasonal fluctuation in volume is a fraction (≈½) of ours. Trossman et al. (2009) put the same argument forward to explain why the Kwon and Riser estimate is rather low. Second, the formal error estimate provided by Kwon and Riser seems rather small. Such a formal error estimate largely depends on the presumed uncertainties, which are not provided or discussed by Kwon and Riser (2004). The various sensitivity tests presented in section 4a suggest that our 2004–06 estimate of $\mathbb{V}_{\mathrm{EDW}}(t)$ does not strongly depend on the choice of data synthesis method. Whether the same is true for the 1961–2001 period and the statistical model that Kwon and Riser (2004) consider remains to be demonstrated. Finally, the extent to which estimates of weakly stratified EDW volumes (such as the one of Kwon and Riser 2004) can be rationalized as part of a precise volume budget framework (such as the one in Walin 1982) remains unclear.

6. Summary and discussion

Based on observations and an observational synthesis (OCCA), a dynamical and quantitative analysis of the EDW layer (defined as all water between 17° and 19°C in the North Atlantic) has been presented for the period from 2004 to 2006. The various observed EDW signals have been brought together using GCM interpolation. We presented the observed signals and showed that they

are well captured in the OCCA observational synthesis. A reference estimate of the volume budget of the EDW layer was presented over the seasonal cycle. Finally, it was shown that this estimate, together with the associated uncertainty estimate, largely resolves apparent conflicts between previous estimates.

The North Atlantic EDW layer outcrop exhibits a pronounced seasonal cycle, covering a 20° latitude range, with isotherms sweeping southward in winter and northward in summer. Worthington (1959)'s depiction of the EDW layer thickness seasonal cycle holds quite well over 2004–06. The EDW layer thickness varies most markedly over a broad region to the south of the Gulf Stream, ranging from about 200 m at the peak of stratification to about 400 m at the peak of convection. This region corresponds to the region where the EDW layer outcrops in winter and the region of large EDW formation rates due to air–sea fluxes, as shown by Maze et al. (2009). The EDW signals described above are consistently established from observations with or without GCM interpolation.

According to our estimates, wintertime increase in EDW volume occurs mostly in February and amounts to 8.6 Svy. Winter formation by air–sea heat fluxes (9.3 Svy) is the leading contribution to this winter EDW volume change. Subsequently, from March through May, air–sea heat fluxes consume 4.6 Svy of the newly formed EDW. Mixing consumes another 2.6 Svy over the year, so that net formation from air–sea fluxes and mixing combined is only 2.0 Svy. It is balanced by EDW volume increase in the North Atlantic (1.4 Svy) mostly, with export from the North Atlantic making a lesser contribution (0.6 Svy). According to our reference estimate, EDW volume is 75 Svy on average over the period from 2004 to 2006 and shows relatively large seasonal fluctuations around this rather stable head of water.

Throughout our sensitivity studies, key quantitative aspects of the seasonal cycle of the EDW layer are found to transcend individual data synthesis approaches, reflecting a robust signal. It was estimated, however, that uncertainties of order ±1.8 Svy prevail in our best available observational estimates of EDW volume budgets based on Argo data. Our reference estimate presents a clear path forward, not only because it covers the full EDW volume budget but also because we associate it with this reasonably conservative error estimate. Large discrepancies beyond ±1.8 Svy among previous estimates were also rationalized.

Acknowledgments. This work was supported by NSF (CLIMODE project), NASA (ECCO2 and ECCO-GODAE projects), and NOPP (ECCO-GODAE project).

APPENDIX

EDW Volume Budget

The procedure used to diagnose the full EDW volume budget [Eqs. (1)–(4); section 3a] for the OCCA reference estimate (section 3b) comprises the following steps:

1) For each grid cell, compute the budget of fluid with $T < \Theta$, for $\Theta = 17°$ and 19°C, as

$$\frac{dv_\Theta}{dt} = a_\Theta - m_\Theta, \tag{A1}$$

where v_Θ, a_Θ, and m_Θ are the volume of $T < \Theta$ fluid inside the grid cell, the grid cell transformation rate at $T = \Theta$, and the export rate of $T < \Theta$ fluid out of the grid cell, respectively.
2) Sum over grid cells in the Atlantic north of 5°N to get

$$\frac{dV_\Theta}{dt} = A_\Theta - M_\Theta. \tag{A2}$$

3) Subtract the volume budget of water with $T < \Theta =$ 17°C from the volume budget of water with $T < \Theta =$ 19°C, to form Eq. (1) and then Eq. (5).

To compute Eq. (A1), two different numerical recipes are used. Their analytical foundation, and practical limitations, will be discussed in detail elsewhere. Here we only outline the numerical recipes.

1) The tracer equation method (TE-M) starts from the grid cell temperature equation,

$$\Delta T/\Delta t \times \Delta V = -\sum_k \mathrm{Nadv}_T^k - \sum_k \mathrm{Adv}_T^k, \tag{A3}$$

where ΔV is the grid cell volume, Δt is the time step, and ΔT is the temperature increment from time t to time $t + \Delta t$; $\{\mathrm{Nadv}_T^k\}$ and $\{\mathrm{Adv}_T^k\}$ are the nonadvective and advective temperature fluxes through the grid cell faces $\{k\}$, counted >0 outward. Equation (A3) is simply converted to Eq. (A1) by multiplying it with

$$\pi_\Theta(T) = \begin{cases} 1/\Delta\Theta, & \Theta^- < T < \Theta^+ \\ 0, & \text{otherwise,} \end{cases} \tag{A4}$$

where T is the grid cell temperature, $\Theta^- = \Theta - \Delta\Theta/2$, $\Theta^+ = \Theta + \Delta\Theta/2$, and $\Delta\Theta$ is a temperature bin. The term $\pi_\Theta(T)$ is a parameterization for the local probability density that the fluid has $T = \Theta$. Hence,

$$\pi_\Theta(T) \times \left(\frac{\Delta T}{\Delta t} \times \Delta V\right),$$

$$\pi_\Theta(T) \times \left(-\sum_k \mathrm{Nadv}_T^k\right), \quad \text{and}$$

$$\pi_\Theta(T) \times \left(-\sum_k \mathrm{Adv}_T^k\right)$$

correspond to dv_Θ/dt, a_Θ, and $-m_\Theta$, respectively.

2) The volume census method (VC-M) starts from the gridcell continuity equation $\sum_k U^k = 0$, where $\{U^k\}$ are the volume fluxes through the gridcell faces $\{k\}$, counted >0 outward. VC-M then uses

$$\Pi_\Theta(T) = \begin{cases} (\Theta^+ - T)/(\Theta^+ - \Theta^-), & \Theta^- < T < \Theta^+ \\ 0, & T > \Theta^+ \\ 1, & T \le \Theta^-, \end{cases} \tag{A5}$$

which is a parameterization of the local concentration of fluid such that $T < \Theta$, to compute dv_Θ/dt as $\Delta\Pi_\Theta/\Delta t \times \Delta V$, followed by $-m_\Theta$ as $-\sum_k U^k \Pi_\Theta^k$ and a_Θ as the residual of Eq. (A1).

Several computational details need elaboration. First, in computing $\pi_\Theta(T)$ and $\Pi_\Theta(T)$, the temperature bin $\Delta\Theta$ must be small compared with the EDW temperature range (19° − 17° = 2°C), so we use $\Delta\Theta = 0.25$°C. The EDW layer edge consists of grid cells where $\pi_{17} \neq 0$ or $\pi_{19} \neq 0$ (forming two discrete isotherms). To avoid scatter in the EDW layer edge, we interpolate temperature fields on to a higher-resolution grid, compute π_Θ and Π_Θ on the refined grid, and then average them back to the native GCM grid. Increasing the resolution by a factor of 12 (in the three directions) was found to be adequate. Second, Eq. (A1) is not computed with $\Delta t = 1$ h (i.e., the GCM time step) to save disk storage. Since the temperature field undergoes rapid evolution (e.g., due to convective mixing), Δt must be small enough to compute Eq. (A1) accurately. It was found that $\Delta t = 1$ day is adequate. Third, all fields necessary to "close" the discrete temperature and volume budgets (needed for TE-M or VC-M) were readily diagnosed by the GCM. For TE-M, $-\sum_k \mathrm{Adv}_T^k$ is the sum of Eulerian and parameterized eddy (GM term; see section 2b) temperature advection terms. The term $-\sum_k \mathrm{Nadv}_T^k$ is the sum of air–sea heat flux terms and parameterized mixing terms (as listed in section 2b; except for the GM term). The sum of air–sea heat flux (mixing) terms leads to an explicit computation of $\overline{\Delta A_{\mathrm{EDW,ext}}}^t$ ($\overline{\Delta A_{\mathrm{EDW,int}}}^t$). There are two "numerical terms" involved: 1) the Adam–Bashforth time stepping, which uses forward extrapolation by half a time step, and 2) the assimilation procedure underlying OCCA, which allows some compensation of model error accumulation (see Forget 2010). Neither one has a clear physical interpretation, but their contributions to Eq. (5) are rather small (<0.3 Svy by year end), so they are simply included as adjustments to $\overline{\Delta A_{\mathrm{EDW,int}}}^t$. For VC-M, $\sum_k U^k$ is the sum of Eulerian and bolus (GM term) velocity contributions. Finally, to go from Eqs. (1)–(4) to Eq. (5), the procedure is 1) compute the 3-yr daily time series of Eqs. (1)–(4), from 1 December 2004 to 30 November 2006; 2) compute the average year daily time series, from 1 December to 30 November; and 3) time integrate to form Eq. (5).

REFERENCES

Adcroft, A., C. Hill, J. Campin, J. Marshall, and P. Heimbach, 2004: Overview of the formulation and numerics of the MIT GCM. *Proc. ECMWF Seminar Series on Numerical Methods: Recent Developments in Numerical Methods for Atmosphere and Ocean Modelling,* Reading, United Kingdom, ECMWF, 139–149. [Available online at http://mitgcm.org/pdfs/ECMWF2004-Adcroft.pdf.]

Fairall, C., E. Bradley, J. Hare, A. Grachev, and J. Edson, 2003: Bulk parameterization of air–sea fluxes: Updates and verification for the COARE algorithm. *J. Climate,* **16,** 571–591.

Forget, G., 2010: Mapping ocean observations in a dynamical framework: A 2004–06 ocean atlas. *J. Phys. Oceanogr.,* **40,** 1201–1221.

Gent, P. R., and J. C. McWilliams, 1990: Isopycnal mixing in ocean circulation models. *J. Phys. Oceanogr.,* **20,** 150–155.

Hanawa, K., and L. Talley, 2001: Mode waters. *Ocean Circulation and Climate,* J. Siedler, J. Church, and J. Gould, Eds., International Geophysics Series, Vol. 77, Academic Press, 373–386.

Kwon, Y., and S. Riser, 2004: North Atlantic subtropical mode water: A history of ocean-atmosphere interaction 1961–2000. *Geophys. Res. Lett.,* **31,** L19307, doi:10.1029/2004GL021116.

Large, W. G., and S. Yeager, 2004: Diurnal to decadal global forcing for ocean and sea-ice models: The data sets and flux climatologies. NCAR Tech. Rep. TN-460+STR, 112 pp.

——, J. C. McWilliams, and S. C. Doney, 1994: Oceanic vertical mixing: A review and a model with a nonlocal boundary layer parameterization. *Rev. Geophys.,* **32,** 363–403, doi:10.1029/94RG01872.

Marshall, J., A. Adcroft, C. Hill, L. Perelman, and C. Heisey, 1997: A finite-volume, incompressible Navier Stokes model for studies of the ocean on parallel computers. *J. Geophys. Res.,* **102** (C3), 5753–5766.

——, D. Jamous, and J. Nilsson, 1999: Reconciling thermodynamic and dynamic methods of computation of water-mass transformation rates. *Deep-Sea Res.,* **46,** 545–572.

——, and Coauthors, 2009: The Climode field campaign: Observing the cycle of convection and restratification over the Gulf Stream. *Bull. Amer. Meteor. Soc.,* **90,** 1337–1350.

Maze, G., G. Forget, M. Buckley, J. Marshall, and I. Cerovecki, 2009: Using transformation and formation maps to study the role of air–sea heat fluxes in North Atlantic Eighteen Degree Water formation. *J. Phys. Oceanogr.,* **39,** 1818–1835.

Reynolds, R., and T. Smith, 1994: Improved global sea surface temperature analyses using optimum interpolation. *J. Climate,* **7,** 929–948.

Siedler, G., A. Kuhl, and W. Zenk, 1987: The Madeira Mode Water. *J. Phys. Oceanogr.,* **17,** 1561–1570.

Speer, K., and E. Tziperman, 1992: Rates of water mass formation in the North Atlantic Ocean. *J. Phys. Oceanogr.,* **22,** 93–104.

Stammer, D., and Coauthors, 2002: The global ocean circulation during 1992–1997, estimated from ocean observations and a general circulation model. *J. Geophys. Res.,* **107,** 3118, doi:10.1029/2001JC000888.

Trossman, D., L. Thompson, K. Kelly, and Y. Kwon, 2009: Estimates of North Atlantic ventilation and mode water formation for winters 2002–06. *J. Phys. Oceanogr.,* **39,** 2600–2617.

Walin, G., 1982: On the relation between sea-surface heat flow and thermal circulation in the ocean. *Tellus,* **34,** 187–195.

Worthington, L., 1959: The 18° water in the Sargasso Sea. *Deep-Sea Res.,* **5,** 297–305.

——, 1976: *On the North Atlantic Circulation*. Johns Hopkins University Press, 110 pp.

Wunsch, C., and P. Heimbach, 2007: Practical global oceanic state estimation. *Physica D,* **230,** 197–208.